International Journal of Solids and Structures 102–103 (2016) 163–175

Contents lists available at ScienceDirect

International Journal of Solids and Structures

journal homepage: www.elsevier.com/locate/ijsolstr

A comparative and parametric study of dynamic cohesive and linear elastic fracture mechanics models

R. Abedi

Department of Mechanical Aerospace and Biomedical Engineering, University of Tennessee Space Institute, 411 B.H. Goethert Parkway, Tullahoma, TN 37355, USA

ARTICLE INFO

Article history:
Received 16 September 2015
Revised 30 July 2016
Available online 17 October 2016

Keywords:
Cohesive fracture
Traction-separation relation
Linear elastic fracture mechanics
Small-scale yielding
Dimensional analysis

ABSTRACT

In cohesive fracture mechanics (CFM), fundamental nondimensional parameters are the ratios of space-time domain geometries and loadings to corresponding intrinsic scales implied by the cohesive fracture traction–separation relations (TSRs). One of these parameters is the nondimensional load-to-strength parameter which is the ratio of the applied loads, expressed in stress form, to an intrinsic strength scale implied by a TSR. Herein the radii of stress singularity from asymptotic Linear Elastic Fracture Mechanics (LEFM) solutions are derived to normalize cohesive process zone (CPZ) sizes from CFM. By approximating these nondimensional CPZ sizes, a simple small-scale yielding (SSY) indicator is derived for dynamic fracture which in turn is shown to be proportional to the square of the load-to-strength parameter. Thus, the load-to-strength parameter serves two purposes. First, increasing this ratio is shown to correspond to more ductile response for families of cohesive fracture self-similar solutions. Second being related to SSY condition, it is used to evaluate the validity of an LEFM model. Numerical results compare characteristic differences between these groups of CFM solutions, investigate the accuracy of the proposed SSY indicator, demonstrate LEFM solutions underestimate crack length and speed even when the SSY condition is satisfied, and study the evolution of the CPZ size.

Published by Elsevier Ltd.

1. Introduction

Cohesive models are among common methods to represent nonlinear material response along a fracture surface. Dugdale (1960) and Barenblatt (1962) proposed the first *cohesive fracture mechanics* (CFM) models. They describe crack initiation and extension by modeling only the gross effects of various nonlinear microscopic damage processes in the neighborhood of the crack tip. Specifically, a constitutive *traction–separation relation* (TSR) describes the tractions acting across a cohesive interface as nonlinear, bounded functions of the interface separation under the assumption that bulk yielding and damage processes are confined to a narrow band along the crack path. At any given instant, these processes are only active along a part of the cohesive interface, called the *cohesive process zone* (CPZ).

Abedi (2010) and Abedi and Haber (2011) derived the set of *fundamental nondimensional parameters* of cohesive fracture mechanics. These parameters are the ratios of various spacetime domain and loading parameters to their intrinsic cohesive fracture counterparts. The load-to-strength parameter $\sigma' = \breve{\sigma}/\tilde{\sigma}$, *i.e.,* the ratio of the applied stress scale $\breve{\sigma}$ to the cohesive reference traction scale $\tilde{\sigma}$, is one of the most important fundamental nondimensional parameters of CFM. The main objective of the present study is to investigate the qualitative and quantitative characterization of cohesive fracture response as σ' varies. It is demonstrated that $\sigma' \propto \sqrt{\Lambda'}$, where the *nondimensional cohesive process zone size* $\Lambda' := \Lambda/\breve{r}$ is the ratio of *cohesive process zone size* Λ to *LEFM stress-singularity radius* $\breve{r}$.

The value of the ratio Λ' is related to the satisfaction of the *small-scale-yielding* (SSY) caveat in *Linear Elastic Fracture Mechanics* (LEFM) theory. Historically, LEFM has served as one of the main tools for modeling and analyzing fracture in solids. However, the singular crack-tip stress fields that are essential to LEFM theory are nonphysical to the extent that yielding or other forms of nonlinear material response act to preclude unbounded stresses within a neighborhood of the crack tip called the *fracture process zone* (FPZ). The SSY condition of LEFM partially addresses this deficiency by requiring that the diameter of the process zone be small relative to the relevant macroscopic length scales, and by acknowledging that the LEFM mechanics fields only hold outside the process zone. Thus, predicting when and identifying the parameters that determine whether the SSY assumption is satisfied are essential for the effective application of LEFM theory.

The verification of SSY is based on the choice of material yielding model as well as the identification of the relevant length

E-mail address: rabedi@utk.edu

http://dx.doi.org/10.1016/j.ijsolstr.2016.10.007
0020-7683/Published by Elsevier Ltd.

scales of the problem. First, simple cohesive models of Dugdale (1960) and Barenblatt (1962), in the context of strip-yield model, have shown to predict the FPZ size well (at least within an order of magnitude) compared to plastic zone models and other nonlinear material models; cf. Dodds Jr et al. (1991) and the references in Anderson (2005). Accordingly, the use of an interfacial cohesive model to represent nonlinear material response is expected to provide accurate estimates for the FPZ size in this work. Second, various length scales such as a finite crack length and the domain diameter have been compared to FPZ size to verify the SSY condition. In view of the finite wave speeds that govern dynamic response, global measures such as crack or domain length scales may not provide meaningful reference length scales. In this work the *stress-singularity radius*, obtained from dynamic LEFM theory, is proposed as an appropriate reference scale for transient, dynamic conditions.

Considering the choices for nonlinear fracture zone Λ and $\check{r}$ for relevant length scale, and noting that $\Lambda' = \Lambda/\check{r} \propto \left(\sigma'\right)^2$ the nondimensional load-to-strength parameter σ' serves two purposes. First, being a CFM fundamental nondimensional parameter, its variation identifies families of self-similar dynamic CFM solutions. Second, its value determines the validity of SSY condition and determines if fracture solutions are acceptable when LEFM theory is employed. That is, by varying the normalized loading ratio, on one hand the families of CFM self-similar solutions are examined, and on the other hand the violation of SSY assumption within LEFM theory is investigated.

It is worth mentioning that the normalization of Λ by a reference length and studying the convergence of CFM to LEFM solutions, as this ratio decreases, has been reported in the literature. For example, Jin and Sun (2005, 2006) define a nondimensional crack length, $a^* \propto a/\Lambda$, *i.e.,* using the inverse of the aforementioned nondimensional CPZ size ratio by using crack length a as the reference length scale, for a cohesive fracture model in a power-law hardening material under quasi-static conditions. They demonstrate good agreement between the LEFM and CFM solutions for large values of a^*. However, to the author's knowledge there has been no studies comparing LEFM and CFM solutions under dynamic condition based on nondimensional variables that are related to the LEFM SSY condition and the CFM nondimensional load-to-strength parameter.

The normalization of Λ by relevant length scales besides checking the validity of the SSY assumption finds applications in closely-related ductile-to-brittle transition in fracture mechanics. Harder (1991) proposes a cohesive length scale, derived from the TSR and bulk constitutive parameters and denoted here by $\tilde{L}$, and defines a *brittleness modulus* in terms of the ratio $a/\tilde{L}$. Carpinteri et al. (2003) propose a nondimensional brittleness indicator; cf. Eq. (15) and (17) in Carpinteri et al. (2003). Although expressed in different terms in Carpinteri et al. (2003) and Abedi and Haber (2011) show that this brittleness indicator can be expressed as, $\tilde{L}/L$, in which L is a characteristic length scale of the analysis domain. Thus, it is equivalent to the reciprocal of Harder's brittleness modulus, except for the substitution of L for a as the reference length scale. Abedi and Haber (2011) also show that $\Lambda \propto \tilde{L}$. Thus, the brittleness indicator of Carpinteri et al. (2003) is proportional to the reciprocal of the SSY indicator, L/Λ, when the SSY condition is satisfied under quasi-static conditions.

The analysis is presented for pure in-plane modes *I* and *II*. In relating modal singular stress-singularity radii $\check{r}_{(k)}$ to model CFM process zone sizes $\Lambda_{(k)}$ the satisfaction of a few conditions are investigated. First, rather than (quasi-)static estimates for fracture process zone size, dynamic estimates such as those in Rice (1968) and Yu and Suo (2000a) are employed to characterize Λ in transient regime. Second, the conditions in which the fracture toughness in the context of LEFM theory can be a good approximation of energy release rate in CFM is discussed.

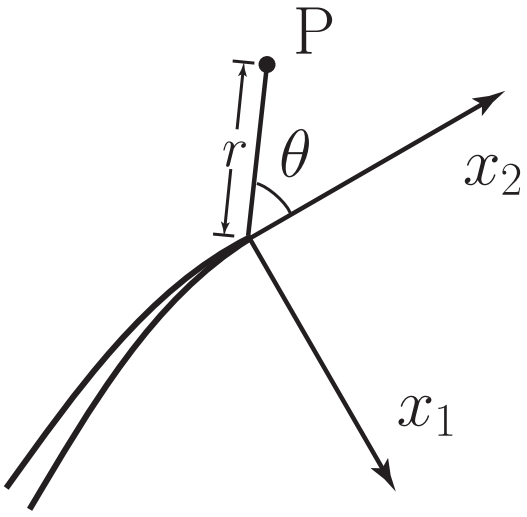

Fig. 1. Local Cartesian and cylindrical coordinate frames moving with a propagating crack tip.

Numerical studies are presented to investigate qualitative and quantitative effect of the nondimensional load σ' on CFM response, including histories of crack tip location and speed. In addition, numerical investigation of the aforementioned conditions, namely the evolution of CPZ size and the energy release rate, are presented. An adaptive spacetime discontinuous Galerkin finite element method (Abedi et al., 2006a,b; 2009) is used in these studies. Various features and properties of the method, such as element-level balance of momentum, simultaneous adaptive control of numerical dissipation and fracture energy error, and linear complexity of the numerical scheme enable to obtain highly accurate and reliable solutions that fully resolve the dynamic evolution of the CPZ.

2. Preliminaries

In this section, the background material needed for the derivation of relevant length scales for LEFM and CFM analyses is provided. Fig. 1 depicts the instantaneous configuration of a moving Cartesian coordinate frame used for both analyses. The local coordinates is denoted by x_i and its origin moves with a propagating crack tip at speed $\hat{v}$ in the x_2-direction; the x_1-direction remains normal to the local crack surface at all times. We shall use $\boldsymbol{e}^k$ to denote unit vectors corresponding to the x_k-directions in the moving frame. The cylindrical coordinates of a point P are (r, θ), in which r is the radial distance from the crack tip and the angle θ is measured counter-clockwise relative to the x_2-axis. The material is assumed to be isotropic. Attention is restricted to domains in two spatial dimensions and to the in-plane fracture modes, $\{I, II\}$, and the special indicial notation, $(k) : k \in \{1, 2\}, (1) = I, (2) = II$, is used to map local coordinate directions, x_k, into normal (I) and tangential (II) modes of cohesive separation. In addition, throughout this paper the summation convention on k and (k) is suppressed.

2.1. LEFM solution at a moving crack tip

Stress solutions from dynamic LEFM theory predict unbounded values near the crack tip, in the limit, as $r \to 0$. These singular fields are fully characterized by the dynamic stress intensity factors, as reviewed below.

2.1.1. Asymptotic expansion of the stress field

The leading term in the asymptotic expansion of the crack-tip stress field is summarized as (Freund, 1990),

$$s^{ij}(r,\theta,t) = \frac{K_I(t)}{\sqrt{2\pi r}}\Sigma_I^{ij}(\theta,\hat{v}) + \frac{K_{II}(t)}{\sqrt{2\pi r}}\Sigma_{II}^{ij}(\theta,\hat{v}) \quad \text{as} \quad r\to 0, \tag{1}$$

where $K_I(t)$ and $K_{II}(t)$ are the *modal dynamic stress intensity factors* for in-plane opening (mode-*I*) and shearing (mode-*II*), $\hat{v}$ is the crack-tip speed, and the components are defined with respect to the moving crack-tip coordinate frame. The stress intensity factors are identified by

$$K_I(t) = \lim_{x_2\to 0}\sqrt{2\pi x_2}s^{11}(x_2,0,t), \quad K_{II}(t) = \lim_{x_2\to 0}\sqrt{2\pi x_2}s^{12}(x_2,0,t). \tag{2}$$

The functions, $\Sigma_I^{ij}(\theta,\hat{v})$ and $\Sigma_{II}^{ij}(\theta,\hat{v})$, describe the angular dependence of the stress components with respect to the moving Cartesian frame as a function of crack-tip speed (Freund, 1990) and are given in Appendix A. Eqs. (1) and (2) imply,

$$\Sigma_I^{11}(0,\hat{v}) = 1, \qquad \Sigma_{II}^{12}(0,\hat{v}) = 1, \tag{3}$$

which is easily verified using (35) and (36) in Appendix A.

The dynamic stress intensity factors can be expressed as (Freund, 1990),

$$K_{(k)}(t,a,\hat{v}) = k_{(k)}(\hat{v})K_{(k)}(t,a,0), \tag{4}$$

in which the *stationary stress intensity factor*, $K_{(k)}(t, a, 0)$, is the stress intensity factor that would result from the same applied loading if the crack tip were stationary at the instantaneous position corresponding to the crack length a, and $k_{(k)}(\hat{v})$ is a universal function of crack-tip speed for mode-(k) crack growth that is independent of the loading and the geometry of the body and that can be approximated as $k_{(k)}(\hat{v}) \approx (1-\hat{v}/c_R)/\sqrt{1-\hat{v}/c_{(k)}}$, where c_R is the Rayleigh wave speed.

The *dynamic energy release rate*, G, which is the rate of mechanical energy outflow from the body into the crack tip per unit crack advance, will be used in subsequent analysis. It can be computed as a function of the instantaneous crack speed and the modal, dynamic stress-intensity factors (Freund, 1990):

$$G = \frac{1-\nu}{2\mu}\left[A_I(\hat{v})K_I^2 + A_{II}(\hat{v})K_{II}^2\right], \tag{5}$$

where

$$A_{(k)}(\hat{v}) = \frac{(1-\alpha_{II}^2)\alpha_{(k)}}{(1-\nu)D} = \frac{\hat{v}^2\alpha_{(k)}}{(1-\nu)c_{II}^2 D}. \tag{6}$$

The functions $A_{(k)}$ are universal functions that do not depend on the details of the loading or on the domain geometry. These functions have the properties, $A_{(k)} \to 1$ as $\hat{v}\to 0^+$ and $A_{(k)} = O[(c_R - \hat{v})^{-1}]$ as $\hat{v}\to c_R$, and are monotone between 0^+ and c_R.

2.2. Analysis of cohesive fracture mechanics

Cohesive interfaces are often added to elastodynamic models to represent crack nucleation and growth. In its most basic form, a cohesive interface is a material surface embedded within the analysis domain across which jumps in the kinematic fields are permitted and the momentum flux is described by a TSR. In this section, the basic concepts of cohesive models are reviewed.

2.2.1. Cohesive traction-separation relations

Let $\tilde{\Gamma}$ denote the collection of all the cohesive interfaces in a given elastodynamic model. A general traction-separation relation can be expressed as,

$$\tilde{\mathbf{t}}(\llbracket\mathbf{u}\rrbracket_{\tilde{\Gamma}};\tilde{\sigma},\tilde{\delta}) = \tilde{\sigma}\mathbf{f}(\tilde{\delta}^{-1}\llbracket\mathbf{u}\rrbracket_{\tilde{\Gamma}}) \tag{7}$$

in which $\tilde{\mathbf{t}}$ is the traction acting across the cohesive interface, $\mathbf{f}$ is a normalized TSR function that relates normalized traction to normalized separation, and $\llbracket\mathbf{u}\rrbracket_{\tilde{\Gamma}}$ is the *cohesive separation* on $\tilde{\Gamma}$. The parameters $\tilde{\sigma}$ and $\tilde{\delta}$ are reference scales for the cohesive traction and the cohesive separation. For example, $\tilde{\sigma}$ is sometimes taken to be the cohesive strength, with $\tilde{\delta}$ the critical cohesive separation that corresponds to $\tilde{\sigma}$ in the TSR or a characteristic separation for which $\tilde{\mathbf{t}}$ vanishes. In the pure mode-*I* and mode-*II* settings discussed in this paper, the corresponding cohesive strength and critical separation are denoted by $\tilde{\sigma}_{(k)}$ and $\tilde{\delta}_{(k)}$, for $k = 1, 2$, respectively. Finally, the modal cohesive works of separation are given by,

$$\tilde{\phi}_{(k)} = \int_0^\infty \tilde{\mathbf{t}}(\xi\boldsymbol{e}^k)\cdot\boldsymbol{e}^k \mathrm{d}\xi = \int_0^\infty \tilde{t}^k(\xi\boldsymbol{e}^k)\,\mathrm{d}\xi. \tag{8}$$

2.2.2. Dimensional analysis of cohesive fracture mechanics

Abedi and Haber (2011) presented the dimensional analysis of CFM. Beside $\tilde{\sigma}$ and $\tilde{\delta}$ which are independent stress and displacement scales of CFM, the analysis yields the complete list of dynamic CFM *intrinsic scales*, including $\tilde{\tau}$, $\tilde{v}$, $\tilde{\phi}$, and $\tilde{L}$ as dimensional scales for time, velocity, the work of separation, time, and length respectively; cf. Eq. (40) in Abedi and Haber (2011) for the description of the complete set of intrinsic scales. Let $\check{\delta}$, $\check{v}$, and $\check{\sigma}$ be displacement, velocity, stress (traction) measures for the load data. Also, let $\check{L}$ and $\check{\tau}$ be length and time measures for the spacetime domain. The ratios, $\check{\delta}/\tilde{\delta}$, $\check{v}/\tilde{v}$, $\check{\sigma}/\tilde{\sigma}$, $\check{L}/\tilde{L}$ and $\check{\tau}/\tilde{\tau}$, are called *fundamental nondimensional parameters of CFM*. A fundamental nondimensional set is defined as a collection of independent, nondimensional parameters having a one-to-one correspondence between families of self-similar solutions and the values of the set. That is, fixing the values of all members of the fundamental set identifies a unique family of self-similar solutions, and any two problems with self-similar solutions must have identical values for all members of the fundamental set. The members of the fundamental set must be independent; that is, no member of the set can be expressed as a function of the other members.

Abedi and Haber (2011) related $\check{L}/\tilde{L}$ to the brittleness indicator from Carpinteri et al. (2003). The ratio $\check{\tau}/\tilde{\tau}$ denotes the importance of various relevant time scales of a problem to the time scale of fracture in the context of CFM. For example, Pandolfi et al. (1999) observe that $\check{\tau}/\tilde{\tau}$ influences the convergence of a time-stepping algorithm for dynamic fracture when $\check{\tau}$ refers to the time step. In this manuscript the influence of the load-to-strength parameter $\sigma' = \check{\sigma}/\tilde{\sigma}$ on CFM self-similar solutions is characterized. Specifically, it is qualitatively and quantitatively demonstrated that as σ' increases CFM solutions further deviate from those predicted from LEFM theory. Another noteworthy and practical outcome of this study is the identification of an effective indicator to verify the validity of the SSY condition in dynamic LEFM.

2.2.3. Geometry of the cohesive process zone

Cohesive models replace a mathematically sharp crack tip with a cohesive process zone (CPZ) that takes the form of a material interface with finite measure, but in general, no clear boundary. The crack-tip position is similarly ill-defined. In the following, the conventions from Abedi et al. (2009) are used to define CPZ geometry in two spatial dimensions. The CPZ size is subsequently used in Section 2.2.4 to derive a nondimensional length parameter.

The *nominal crack-tip position* is defined as the location where the critical cohesive separation $\tilde{\delta}$ is attained. The *trailing edge of the CPZ* is the position behind the crack tip where the cohesive tractions first vanishes. If this location is not well defined, the trailing edge is identified with the location where $\llbracket\mathbf{u}\rrbracket_{\tilde{\Gamma}} = \delta_T > \tilde{\delta}$, in which δ_T is the separation at which the cohesive traction falls to 1% of the strength $\tilde{\sigma}$. In general, the leading edge of the CPZ is identified

by the condition, $[\![\mathbf{u}]\!]_{\tilde{\Gamma}} = \delta_{\mathrm{L}}$, where δ_{L} is the smallest cohesive separation at which significant crack-like behavior (*i.e.,* large strains and velocities) is observed. Following common practice, δ_{L} is set to $\delta_{\mathrm{L}} = \tilde{\delta}$.

In the present two-dimensional setting, the *nominal CPZ* is the segment of the cohesive interface between the leading and trailing edges, and *CPZ size*, denoted by Λ, is defined as the distance between the leading and trailing edges. Although there is a level of arbitrariness in these definitions, reasonable alternative definitions for the leading and trailing edges generally scale Λ by a factor that is only $\mathcal{O}(1)$. The modal CPZ sized are denoted by $\Lambda_{(k)}$, where $\tilde{\sigma}_{(k)}, \tilde{\delta}_{(k)}$ and the corresponding modal traction and separation values are used to determine the positions of the leading and trailing edges.

2.2.4. Estimates for modal cohesive process zone sizes

There are several estimates in the literature for modal process-zone sizes under quasi-static conditions (Rice, 1968, 1980). For isotropic materials they can be presented in the combined form,

$$\Lambda^0_{(k)} = \zeta_{(k)}\pi \frac{\mu}{1-\nu}\frac{\tilde{\phi}_{(k)}}{(\tilde{\sigma}_{(k)})^2}, \tag{9}$$

in which the superscript '0' indicates a quasi-static value. The value of the scalar factor $\zeta_{(k)}$ depends on the choice of TSR and on the convention employed in the definition of process-zone size. For instance, Rice estimated $\zeta_{(1)} = 1/4$ for the Dugdale model (Rice, 1968), and proposed $\zeta_{(1)} = 9/16$ for potential-based TSRs (Rice, 1980).

One can show, using the methods advanced in Freund (1990) and Yu and Suo (2000b) and subject to the SSY condition and steady crack-growth conditions, that for any extrinsic cohesive model,

$$\Lambda_{(k)} = \frac{\Lambda^0_{(k)}}{A_{(k)}(\hat{v})}. \tag{10}$$

in which $A_{(k)}$ are the crack-speed-dependent universal functions given in (6). Then, combining (9) and (10), we obtain,

$$\Lambda_{(k)} = \zeta_{(k)}\pi \frac{\mu}{1-\nu}\frac{\tilde{\phi}_{(k)}}{(\tilde{\sigma}_{(k)})^2 A_{(k)}(\hat{v})}. \tag{11}$$

In view of the behavior of $A_{(k)}(\hat{v})$ (cf. discussion in Section 2.1), (11) implies that the CPZ size approaches zero as $\hat{v} \to c_{\mathrm{R}}$. Yu and Suo (2000b) obtained results for more general crack velocities and loadings that agree with the results in (9) and (10). In Section 5.3 we discuss the accuracy of the estimate (11) and its implication on the validity of an SSY indicator proposed in Section 3.3.

3. Analysis

In this section stress-singularity radii are proposed as reference length scales for LEFM theory. In comparison to modal CPZ-size estimates from Section 2.2.4, meaningful nondimensional forms for CPZ-sizes and modal SSY criteria are introduced. By introducing an energetic approximation, the aforementioned nondimensional CPZ sizes are related to nondimensional load-to-strength parameter σ'. This result not only provides a means to quantify the differences between the solution of families of CFM self-similar problems, as σ' is varied, but also provides modal SSY indicators that can be evaluated directly from problem data without the need for an expensive nonlinear analysis. The numerical studies reported in Section 5 demonstrate the variation of CFM self-similar solutions as σ' is varied and, despite the approximations, support the reliability of the proposed SSY indicators for the LEFM theory.

3.1. LEFM modal stress-singularity radii

Asymptotic analyses in dynamic LEFM generally represent problems involving far-field loads acting on cracked bodies as superpositions of two simpler subproblems (Freund, 1990). Here this decomposition is used to develop estimates of the regions where singular response dominates in LEFM stress solutions. In the first subproblem, the far-field loading acts on an uncracked body with geometry and material properties that are otherwise identical to the original cracked body. The second subproblem involves the cracked geometry subjected to traction loads that cancel the crack-face tractions generated by the stress solution from the first subproblem. The superposition of the two subproblems provides, by construction, a solution that satisfies the traction-free condition on the crack faces. If, in addition to far-field loads, the original problem involves tractions that act directly on the evolving crack faces, then these loads are added to the second subproblem.

Since the solution to the first subproblem is bounded, the singular response of the original system resides entirely in the solution to the second subproblem. Thus, only the second subproblem is considered in asymptotic studies of the crack-tip fields. Eq. (1) gives the leading singular term in the asymptotic expansion of the crack-tip stress field, which is $\mathcal{O}(r^{-1/2})$. The second term in the expansion is spatially uniform, and therefore zeroth-order in r. For very small values of r, the singular term dominates the stress solution. However, as r increases, the singular term trends toward zero, so that the zeroth-order term, and eventually higher-order terms, become dominant.

We are interested in quantifying the critical radii below which the singular terms dominate the rest of the stress solution, and we refer to these as the *LEFM stress-singularity radii*. In general, these radii vary with the angle θ. However, it is convenient and sufficient to consider only $\theta = 0$, *i.e.,* the direction directly ahead of the crack tip, to establish an overall scale for the singular zone. In particular, $\breve{r}_{(k)}(t)$ is used to denote the stress-singularity radius for mode-(k) at time t for $\theta = 0$. Let $\breve{\sigma}_k(t); k = 1, 2$ denote the limiting values, as $r \to 0$, of the normal and tangential components of the prescribed crack-face tractions in the second subproblem. It turns out that these limiting values determine the zeroth-order terms in the asymptotic expansions for the normal components of the crack-tip stress field (*i.e.,* s^{11} and s^{12}) (Freund, 1990). That is, $s^{1k}_0(t) = \breve{\sigma}_k(t)$, in which a subscript '0' indicates a zeroth-order term in an asymptotic expansion.

The modal stress-singularity radii are identified by equating the leading singular terms, evaluated at $(r, \theta, t) = (\breve{r}_{(k)}(t), 0, t)$ with the corresponding zeroth-order terms. Then, recalling (1) and (3), we have

$$\frac{|K_{(k)}(t)|}{\sqrt{2\pi\breve{r}_{(k)}(t)}}|\Sigma^{1k}_{(k)}(0,\hat{v})| = \frac{|K_{(k)}(t)|}{\sqrt{2\pi\breve{r}_{(k)}(t)}} = |\breve{\sigma}_k(t)|$$
$$\Rightarrow \breve{r}_{(k)}(t) := \frac{1}{2\pi}\left(\frac{K_{(k)}(t)}{\breve{\sigma}_k(t)}\right)^2. \tag{12}$$

It is worth mentioning the relation between singular radii with other closely related length scales from LEFM theory. First when the nonlinear behavior around the crack tip is modeled by plasticity, the plastic zone size r_p is estimated by a variety of approaches such as Irwin or strip yield models; cf. (Anderson, 2005) and also the discussion on (22) in Section 3.3. With these models we have $r_{p_{(k)}} \propto (K_{(k)}/\sigma_{\mathrm{Y}})^2$ where σ_{Y} is the yield stress. Clearly, $r_{p_{(k)}}$ is distinct from $\breve{r}_{(k)}$ and has a different physical interpretation. Second, another length scale can be derived from the T-stress. T-stress is the zeroth order term of the normal stress parallel to the x_2-axis, *i.e.,* $T(t) = s^{22}_0(t)$. The interaction of T-stress and $K_{(k)}$ introduces two other length scales $\breve{r}^T_{(k)}(t) = \frac{1}{2\pi}(K_{(k)}(t)/T(t))^2$. Since T-stress does not induce a traction on crack surfaces and $\breve{\sigma}_k(t)$ are related

to (equivalent) crack surface tractions, $s_0^{1k}(t) = \breve{\sigma}_k(t)$, the singular radii in (12) are not related to $\breve{r}^T_{(k)}(t)$. However, as demonstrated by Cornetti et al. (2014) a nondimensional length scale derived from $\breve{r}^T_{(k)}$, *i.e.*, by dividing it by the crack length a, finds application in *finite fracture mechanics* (FFM), where a stress-based criterion is added to conventional energy-based LEFM crack propagation criterion.

From here on, the temporal arguments of $\breve{r}_{(k)}$ and $\breve{\sigma}_k$ are suppressed for convenience. The stress-singularity radii are compared with CPZ size in Section 2.2.4 to form dimensionless indicators for satisfaction of the SSY condition under dynamic conditions. It is convenient to rewrite (12) in terms of the dynamic energy release rate, G. A relation between $\breve{r}_I$ and $\breve{r}_{II}$, for general mixed-mode loading, can be obtained by combining (12) and (5). However, we are more interested in the pure mode-*I* and mode-*II* cases, cf. Section 2.2, where by using (5) the modal radii of singularity are obtained as,

$$\breve{r}_{(k)} = \frac{1}{\pi\,(1-\nu)}\,\frac{\mu G_{(k)}}{A_{(k)}(\hat{v})\breve{\sigma}_k^2}. \tag{13}$$

in which the subscript on G indicates a modal energy release rate.

3.2. Normalization of modal CPZ-sizes

To derive nondimensional CPZ sizes, modal CPZ sizes are normalized by their corresponding modal LEFM singular radii to obtain,

$$\Lambda'_{(k)} := \frac{\Lambda_{(k)}}{\breve{r}_{(k)}} \tag{14}$$

which are basically proportional to the nondimensional length scales $\tilde{L}/\breve{L}$ in Section 2.2.2 for $\breve{L} = \breve{r}_{(k)}$ given that $\Lambda_{(k)}$ from (11) is proportional to CFM length scale $\tilde{L}$; cf. (Abedi and Haber, 2011).

Unfortunately, the quantities, $\Lambda_{(k)}$ and $\breve{r}_{(k)}$ in (14) depend on the crack-tip speed and are difficult to compute individually. Herein, the CPZ-size estimate (11) is used for $\Lambda_{(k)}$ in (14). Given the same dependence of $\breve{r}_{(k)}$ and $\Lambda_{(k)}$ on crack speed $\hat{v}$ through the term $A_{(k)}(\hat{v})$ in (11) and (13) the ratios $\Lambda'_{(k)}$ are expressed as,

$$\Lambda'_{(k)} = \frac{\Lambda_{(k)}}{\breve{r}_{(k)}} = \zeta_{(k)}\pi^2\,\frac{\tilde{\phi}_{(k)}}{G_{(k)}}\left(\frac{\breve{\sigma}_k}{\tilde{\sigma}_{(k)}}\right)^2, \tag{15}$$

Although the estimate (11) is based on an assumption of steady-state crack propagation, it is expected to remain valid for unsteady crack speeds when the CPZ size is small compared to the overall crack length and when the normalized crack speed, $\hat{v}/c_{\mathrm{R}}$, does not change appreciably during crack extensions on the order of the CPZ-size (Freund, 1990). The numerical results in Section 5 support this expectation under typical conditions and suggest that these relations also hold for intrinsic cohesive models. However, (11) loses accuracy as either the SSY condition or the above condition on normalized crack speed is violated. Even in these extreme situations, the relation between CPZ size and crack-tip speed is qualitatively similar to the one predicted by (11). This matter is discussed in more detail in Section 5.3.

Next it is shown that, under certain conditions, the ratio $\tilde{\phi}_{(k)}/G_{(k)}$ is well approximated by unity to obtain a useful estimate for the normalized CPZ size from (14). If it is assumed that the SSY assumption holds, then the *modal dynamic energy release rates* for an extrinsic cohesive model are given by Freund (1990),

$$G_{(k)} = \frac{1}{\hat{v}}\int_{-\Lambda_{(k)}}^{0} \tilde{t}^k(\delta_k \boldsymbol{e}^k)\,\frac{\partial \delta_k}{\partial t}\,\mathrm{d}x_2 + \tilde{\phi}_{(k)} = I_{(k)} + \tilde{\phi}_{(k)}, \tag{16}$$

in which δ_k are values of the separation components, defined with respect to the crack-tip Cartesian frame as functions of x_2 along the cohesive interface, and the cohesive work of separation, $\tilde{\phi}_{(k)}$, is defined in (8).[1]

The integrals $I_{(k)}$ in (16) represent the transient contributions of the modal separation rates, as observed in the moving crack-tip frame. They vanish identically when the crack speed is steady. In this case, we obtain $G_{(k)} = \tilde{\phi}_{(k)}$. The contribution of $I_{(k)}$ can also be neglected under transient conditions as $\hat{v} \to c_{\mathrm{R}}$, since then $\Lambda_{(k)} \to 0$ (cf. Section 2.2.4). In fact, employing the estimate for the CPZ size (11) we get,

$$\left|\frac{I_{(k)}}{\tilde{\phi}_{(k)}}\right| \le \frac{\tilde{\sigma}_{(k)}\Lambda_{(k)}}{\hat{v}\tilde{\phi}_{(k)}}\left\|\frac{\partial \delta_k}{\partial t}\right\|_\infty \approx \frac{\zeta_{(k)}\pi\mu}{(1-\nu)\hat{v}A_{(k)}(\hat{v})\tilde{\sigma}_{(k)}}\left\|\frac{\partial \delta_k}{\partial t}\right\|_\infty. \tag{17}$$

where $|I_{(k)}| = \left|\frac{1}{\hat{v}}\int_{-\Lambda_{(k)}}^{0}\tilde{t}^k(\delta_k\boldsymbol{e}^k)\frac{\partial\delta_k}{\partial t}\,\mathrm{d}x_2\right| \le \frac{1}{\hat{v}}\int_{-\Lambda_{(k)}}^{0} ||\tilde{t}^k(\delta_k\boldsymbol{e}^k)||_\infty\, ||\frac{\partial\delta_k}{\partial t}||_\infty\,\mathrm{d}x_2 = \Lambda_{(k)}\left(\tilde{\sigma}_{(k)}\left\|\frac{\partial\delta_k}{\partial t}\right\|_\infty\right)/\hat{v}$ is used in the derivation of (17). The upper bound in (17) vanishes, in the limit, as $\hat{v} \to c_{\mathrm{R}}$, due to the properties of $A_{(k)}$. Consequently, while $I_{(k)}$ can contribute a significant part of $G_{(k)}$ at small crack speeds, it can be ignored at higher crack velocities. That is, approximating $G_{(k)}$ with $\tilde{\phi}_{(k)}$ is well justified, except when $\hat{v}/c_{\mathrm{R}} \ll 1$. Furthermore, numerical studies show that this ratio is, in general, $\mathcal{O}(1)$ (cf. Section 5.2). Subject to this restriction, the main factors that determine $\Lambda'_{(k)}$ in (15) are the modal nondimensional load intensities, $\breve{\sigma}_k/\tilde{\sigma}_{(k)}$, in which the limiting tractions and the modal cohesive-traction scales can typically be computed from prescribed data. Thus, by the use of the justified substitution $\tilde{\phi}_{(k)}/G_{(k)} \to 1$ for pure mode k in (15), we define,

$$\lambda'_{(k)} = \zeta_{(k)}\pi^2\left(\frac{\breve{\sigma}_k}{\tilde{\sigma}_{(k)}}\right)^2, \quad \text{where} \quad \Lambda'_{(k)} \approx \lambda'_{(k)}. \tag{18}$$

3.3. Modal SSY indicators

In the context of cohesive models for dynamic fracture response, the SSY condition of LEFM requires that the modal CPZ sizes, $\Lambda_{(k)}$, be much smaller than all other relevant length scales of the model. Applying this principle to the modal stress-singularity radii defined in Section 3.1, we propose,

$$\Lambda'_{m(k)} := \max_{t\in\mathcal{I}}\Lambda'_{(k)} = \max_{t\in\mathcal{I}}\frac{\Lambda_{(k)}}{\breve{r}_{(k)}} \ll 1, \tag{19}$$

in which $\mathcal{I}$ is the analysis time interval of interest, as a suitable nondimensional criterion for SSY in LEFM under dynamic conditions. As the ratio, $\Lambda'_{(k)} = \Lambda_{(k)}/\breve{r}_{(k)}$ falls below unity, the CPZ becomes smaller than the zone where the stress-singularity dominates, and the LEFM theory gains accuracy. In contrast to SSY indicators developed for quasi-static response that use global length scales derived from the crack or domain geometry, the stress-singularity radii are local scales associated with the crack-tip fields, consistent with the finite wave speeds that govern dynamic response. If during the relevant time scales of the problem, global length scales interfere with crack tip stress field, they also must be taken into account for the verification of SSY condition.

Given the strong dependence of $\Lambda_{(k)}$ and $\breve{r}_{(k)}$ on crack-tip speed and the presence of $\frac{\tilde{\phi}_{(k)}}{G_{(k)}}$ in the value of $\Lambda'_{(k)}$ in (15) the approximation (18), based on $\tilde{\phi}_{(k)}/G_{(k)} \approx 1$ from Section 3.2, is employed to develop an SSY indicator that is easy to evaluate using only the problem data. This new indicator provides a convenient means

[1] In Freund (1990), the upper limit of integration in the integral for $\tilde{\phi}_{(k)}$ is δ_{T}, the nominal separation at which the cohesive tractions vanish, rather than ∞, as in (8). The effect of this difference should be negligible if the cohesive tractions at δ_{T} are suitably small.

to identify conditions under which the SSY assumption holds and, therefore, LEFM models of dynamic fracture are valid. Based on this approximation, the *modal nondimensional SSY indicators*, denoted by $\lambda'_{m(k)}$, and the associated *modal SSY conditions* are defined as,

$$\lambda'_{m(k)} := \max_{t\in\mathcal{I}} \lambda'_{(k)} = \zeta_{(k)}\pi^2 \max_{t\in\mathcal{I}} \left(\frac{\check{\sigma}_k}{\tilde{\sigma}_{(k)}}\right)^2 \ll 1. \tag{20}$$

Eq. (20) provides practical a priori tests of whether the SSY condition is satisfied for modes-(k) in dynamic CFM.

Relations similar to (20) can be found in the literature. Freund (1990) studies the problem of a uniform tensile stress impinging on a crack within an infinite, elastic–perfectly-plastic domain with yield strength σ_Y. The stress loading generates a plastic zone around the crack tip whose radius along the crack direction, r_p, can be computed from,

$$\frac{r_p}{c_d t} = \frac{1-2\nu}{2(1-\nu)^2}\left(\frac{\check{\sigma}}{\sigma_Y}\right)^2. \tag{21}$$

Similar to (20), the radius of inelastic response is proportional to the ratio of a loading measure to the material's strength. It is worthwhile to contrast the proposed SSY indicator (20) for dynamic CFM with (21) and to note the distinctions between the underlying models for inelastic material response; a TSR-based cohesive model is used for the former and perfect plasticity for the latter.

Finally, combining (21) with the expression for the stress intensity factor for this particular loading, cf. (26), we obtain

$$r_p = \frac{\pi}{8}\left(\frac{K_I(t,a,0)}{\sigma_Y}\right)^2, \tag{22}$$

which is the elastodynamic generalization of the well-known result for the plastic-zone size based on the strip-yield model (Rice, 1968). The SSY condition for this case requires that r_p is small compared to the other relevant length scales of the model.

3.4. Relation between SSY indicator and CFM nondimensional analysis

Let $\check{\sigma}$ be a stress-valued measure of the load data. As discussed in Section 2.2.2 $\sigma' := \check{\sigma}/\tilde{\sigma}$ is one of the fundamental nondimensional parameters associated with cohesive fracture mechanics. For a given mixture of modal loads, we have $\check{\sigma}_k \propto \check{\sigma}$, so the modal stress ratios in (20), $\check{\sigma}_k/\tilde{\sigma}_{(k)}$, are also fundamental parameters. Thus, any specific set of values for $\check{\sigma}_k/\tilde{\sigma}_{(k)}$ and the other fundamental parameters describes an infinite family of problems with self-similar solutions. Solutions to problems with distinct values for any of the modal stress ratios are not self-similar.

Increasing the load-to-strength parameter σ' has three related interpretations. First, this results in a squarely proportional increase to $\Lambda/\check{r}$, cf. (18), implying a more ductile response based on the definition of brittleness indicator in Section 1. Second, the SSY indicator λ'_m from (20) increases in a similar fashion. That is, when σ' increases LEFM theory loses accuracy and as expected fracture response becomes more ductile. Finally, this brittle-to-ductile transition classifies how solutions corresponding to distinct ratios σ' conceptually differ within CFM.

4. Solution schemes for a reference problem in an infinite domain

This section presents the approaches used to obtain LEFM and CFM solutions for a mode I problem in an infinite domain. A semi-analytical approach is used for the solution of LEFM problem, while the CFM problem is solved with the spacetime discontinuous Galerkin method. The numerical results and their interpretation are subsequently presented in Section 5.

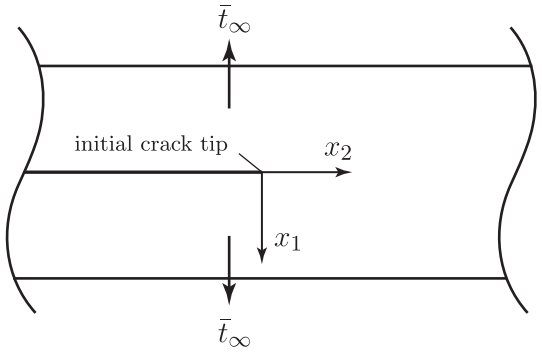

Fig. 2. Domain and load description for a plate containing a half-plane crack.

Consider dynamic propagation of a semi-infinite crack in an infinite domain, as depicted in Fig. 2. The spatial coordinates $(x_1, x_2) \in \mathbb{E}^2$ is defined such that the x_1-direction is normal to the crack plane described by $x_1 = 0$, and the crack surface coincides with the negative part of the x_2-axis at the initial time when the crack tip is at the origin of the spatial coordinate system. Traction-free conditions are prescribed on the crack faces at all times and a spatially uniform, mode-I traction, $\bar{t}_\infty$, is applied as the far-field loading. The far-field tractions act suddenly and generate sharp wavefronts that approach the crack plane from both sides to arrive at time $t = 0$.

A material model is used that approximates the elastic properties of polymethyl methacrylate (PMMA): Young's modulus, $E = 3.24$ GPa; Poisson's ratio, $\nu = 0.35$; and mass density, $\rho = 1190$ kg/m^3. For these values of the material parameters, the dilatational, shear and Rayleigh wave speeds are $c_d = 2090$ m/s, $c_s = 1004$ m/s, and $c_R = 938$ m/s. Since the results are presented in nondimensional form, the values of individual dimensional quantities are less significant than the nondimensional parameters that are derived from them.

In view of the unbounded domain and crack geometry, commonly-used macroscopic length scales, such as a characteristic dimension of the spatial domain or the crack length a, are unavailable in this example, as is a natural time scale. Therefore, SSY or brittleness indicators based on macroscopic scales, such as those in Jin and Sun (2005, 2006), Harder (1991) and Carpinteri et al. (2003), are not appropriate for this example. In fact, the stress-singularity radii introduced in Section 3.1 are the only reference length scales available to characterize the cohesive fracture problem. All other members of the fundamental nondimensional set listed in Abedi and Haber (2011) either vanish in this example or are unavailable due to the unbounded domain. Thus, the normalization of the CPZ-size given in (14), and the decision to limit the scope of the parametric study to the fundamental parameter that governs the traction-loading amplitude is not restrictive.

The results reported in Section 3, including the SSY indicator $\lambda'_{m(k)}$, are general for fracture modes I and II in two-dimensional domains. The reference solution examined is, however, only concerned with pure mode-I response, so from here on modal indices are suppressed in all mathematical expressions.

4.1. Reference LEFM solution

This section presents a semi-analytical LEFM solution for the model problem. First the decomposition of the crack face tractions in nondimensional form as well as the history of the corresponding stationary stress intensity factor, cf. (4), are developed. Then Grif-

fith's criterion is introduced for crack propagation and the analysis of the resulting crack-tip dynamics.

4.1.1. Crack-face tractions and stationary stress intensity factor

The LEFM solution for the model problem is computed from the superposition of two subproblems; cf. Section 3.1. In the first subproblem, the far-field loading acts on the un-cracked body, and additive interference between the two incident waves generates a spatially uniform tensile stress, $2H(t)\bar{t}_\infty$, on the entire $x_1 = 0$ plane. Thus, the stress intensity factor for the first subproblem is zero. In the second subproblem, which has the same cracked geometry as the original problem, compressive tractions with intensity

$$\bar{t}(t) = 2H(t)\bar{t}_\infty \tag{23}$$

act uniformly on the crack faces, so that $\bar{t}_\infty$ determines the stress intensity factor for $t > 0$; cf. Section 2.1. Furthermore, the limiting magnitude of the compressive traction acting on the trailing faces of the crack, as $r \to 0$, is simply, $\breve{\sigma}(t) = \bar{t}(t)$. The Heaviside function $H(t)$ in (23) takes the value of one for $t \geq 0$ and zero otherwise. The scale of the traction loading for the second subproblem is $\breve{\sigma} = 2\bar{t}_\infty$ (cf. Section 2.2.2). The *normalized load intensity* is defined as,

$$\sigma' := \frac{\breve{\sigma}}{\tilde{\sigma}} = 2\frac{\bar{t}_\infty}{\tilde{\sigma}} \quad \Rightarrow \quad \frac{\breve{\sigma}(t)}{\tilde{\sigma}} = \frac{\bar{t}(t)}{\tilde{\sigma}} = 2H(t)\frac{\bar{t}_\infty}{\tilde{\sigma}} = \sigma' H(t). \tag{24}$$

Together, Eqs. (15) and (24) imply that the normalized load intensity σ' governs the size ratio, $\Lambda/\breve{r}$. This prediction is tested using numerical estimates for the process-zone size, Λ, in Section 5.

For the present case of spatially uniform, mode-*I* loading impinging on a stationary crack face, we have (Freund, 1973),

$$K(t, a, 0) = C\sqrt{2\pi c_\mathrm{d}}\int_{-\infty}^{t} \bar{t}'(z)\sqrt{t - z}\,\mathrm{d}z, \tag{25}$$

where $C = \sqrt{2(1-2\nu)}/\pi(1-\nu) = 2c_\mathrm{s}/(\pi c_\mathrm{d}\sqrt{1-\nu})$ and $\bar{t}'$ is to be interpreted as a distributional derivative. For the step-function loading, (23), one finds

$$K(t, a, 0) = C\sqrt{2\pi c_\mathrm{d} t}\,\breve{\sigma}. \tag{26}$$

4.1.2. Crack-tip kinetics

In order to predict the trajectory of a moving crack with LEFM theory, the governing equations must be augmented with an extrinsic *crack-growth criterion* or *crack-tip equation of motion*. The accuracy of the resulting LEFM model, relative to either real material response or a more detailed nonlinear model, depends on both the satisfaction of the SSY condition and the suitability of the chosen crack-growth criterion. The most common criterion is the *generalized Griffith's critical energy-release-rate criterion*, which states that a crack can only grow when the dynamic energy release rate equals the material's fracture energy. In the simplest material description, the energy required per unit area of new crack surface is a constant, denoted by Γ_0, called the *specific fracture energy*. Consequently, the LEFM crack-tip equation of motion takes the simple form,

$$G = \Gamma_0. \tag{27}$$

Next, (27) is used to analyze the LEFM crack-tip kinetics for the model problem. Eqs. (4) and (27) yield,

$$\frac{1-\nu}{2\mu}A(\hat{v})k(\hat{v})^2[K(t, a, 0)]^2 = \Gamma_0 \tag{28a}$$

$$\Leftrightarrow \quad g(\hat{v}) = \frac{2\mu\Gamma_0}{(1-\nu)[K(t, a, 0)]^2}, \tag{28b}$$

where $g(\hat{v}) := A(\hat{v})k(\hat{v})^2$ is a universal function of the crack-tip speed that is very accurately approximated by $g(\hat{v}) \approx 1 - \hat{v}/c_\mathrm{R}$ for $0 \leq \hat{v} \leq c_\mathrm{R}$. In view of (25), and recalling that $H'(t) = \delta_0$, the crack-tip equation of motion for this special loading reduces to

$$g(\hat{v}) = \frac{\mu\Gamma_0}{(1-\nu)\pi c_\mathrm{d}(C\breve{\sigma})^2 t}. \tag{29}$$

As time increases, the right-hand side of (29) approaches unity from its initial, unbounded value. The crack remains stationary while this quantity is greater than unity and crack growth initiates at a critical time, denoted by τ_0, when it reaches unity, since $g(\hat{v}) = 1$ for a stationary crack. This is the instant when, for the first time, (27) can be satisfied, since $G < \Gamma_0$ for earlier times. The right-hand side of (29) equals unity when

$$\tau_0 = \frac{\pi\mu\tilde{\phi}c_\mathrm{d}}{4(c_\mathrm{s}\breve{\sigma})^2}, \tag{30}$$

in which $\tilde{\phi}$ is substituted for Γ_0, as justified by the discussion below (27).

Noting that $g(\hat{v}) \approx 1 - \dot{a}/c_\mathrm{R}$, we obtain

$$\dot{a}' = \begin{cases} 0 & : \quad 0 < t' \leq 1 \\ 1 - \frac{1}{t'} & : \quad 1 < t' \end{cases} \tag{31a}$$

$$a' = \begin{cases} 0 & : \quad 0 < t' \leq 1 \\ t' - 1 - \ln t' & : \quad 1 < t' \end{cases} \tag{31b}$$

in which $\dot{a}' := \dot{a}/c_\mathrm{R}$, $a' := a/\tau_0 c_\mathrm{R}$ and $t' := t/\tau_0$ are normalized, nondimensional values for the crack-tip speed, crack-tip position and time. It is observed that $\dot{a}'$ approaches unity asymptotically as $t' \to \infty$ and that $\tau_0 \propto 1/(\breve{\sigma})^2$.

In the present setting, CFM serves as the reference model for nonlinear material response. In contrast to LEFM models, where extrinsic crack-growth criteria are required, the intrinsic cohesive constitutive properties govern the crack-tip kinetics in CFM theory. In order to validate the proposed CPZ-size estimate and SSY indicator by comparing LEFM and CFM response, the LEFM model must be calibrated to obtain a good match between the two models when it is expected. Eq. (16) implies that $G = \tilde{\phi}$ under steady crack-growth conditions and that $G \to \tilde{\phi}$ as $\hat{v} \to c_\mathrm{R}$; cf. Section 3.3. Although these results do not cover all possible regimes where SSY holds, nonetheless $G = \tilde{\phi}$ is combined with (27) to obtain $\Gamma_0 = \tilde{\phi}$ and to test the agreement between the resulting LEFM model and the CFM model numerically, as reported below.

4.2. Numerical model for the CFM theory

4.2.1. Cohesive traction–separation relation

The history-independent, exponential TSR developed by Xu and Needleman (1994) is used to model the cohesive fracture process. In the interest of simplicity, but without loss of generality, the critical separations and the works of separation are assumed to be equal for the normal and tangential directions; cf. (Xu and Needleman, 1994). That is, $\tilde{\delta}_{(1)} = \tilde{\delta}_{(2)} := \tilde{\delta}$ and $\tilde{\phi}_{(1)} = \tilde{\phi}_{(2)} := \tilde{\phi}$. The function $\mathbf{f}$ in (7) then takes the form, cf. (Abedi et al., 2009),

$$\mathbf{f}\begin{pmatrix} [\![u_1]\!] \\ [\![u_2]\!] \end{pmatrix} = \begin{pmatrix} \Delta_1 \exp\left(1 - \Delta_1 - \Delta_2^2\right) \\ 2\Delta_2(1+\Delta_1)\exp\left(1 - \Delta_1 - \Delta_2^2\right) \end{pmatrix}, \tag{32}$$

in which $\Delta_1 := [\![u_1]\!]/\tilde{\delta}$ and $\Delta_2 := [\![u_2]\!]/\tilde{\delta}$ are, respectively, normalized separations in the normal and tangential directions. In this particular case, the normal cohesive strength, $\tilde{\sigma}$, is achieved for $[\![u_1]\!] = \tilde{\delta}$. That is, $\tilde{\sigma}$ and $\tilde{\delta}$ in (7) are the cohesive strength and the critical separation for the normal direction. The work of separation is

$$\tilde{\phi} = e\tilde{\sigma}\tilde{\delta}, \tag{33}$$

in which $e \approx 2.718$ is the natural log base. The nominal crack-tip position, defined according to the conventions introduced in

Section 2.2.3, moves in the positive x_2 direction. Therefore, the TSR is applied along the potential crack path, defined as the set $\{(x_1, x_2) : x_1 = 0, x_2 > 0\}$.

The cohesive parameters used in the computations are based on those in Xu and Needleman (1994): $\tilde{\sigma} = 0.1E = 324$ MPa and $\tilde{\delta} = 4.0 \times 10^{-4}$ mm. However, since the results are presented in terms of nondimensional variables, alternative choices for the cohesive and material parameters, other than Poisson's ratio, would not affect the results (Abedi and Haber, 2011).

4.2.2. Finite element discretization

The spacetime discontinuous Galerkin (SDG) method described in Abedi et al. (2006a,b; 2009) is used to approximate the response of the CFM model. Although the details of the SDG finite element method are not the primary concern in this work, it is noted that the method's element-wise balance properties, linear scaling properties, unique spacetime adaptive meshing capabilities, and use of two adaptive error indicators (one that limits spurious numerical dissipation in the bulk material and one that measures the residual of the TSR on the cohesive interface (Abedi et al., 2009)) combine to provide exceptionally high precision in the numerical results reported here. For example, Xu and Needleman (1994) reported numerical crack velocities that exceeded the Rayleigh speed for high values of σ'. This problem was not encountered in the present study. Even for σ' as high as $10^{-1/128}$, the crack speeds were bounded by the Rayleigh wave speed.

While there are various specialized techniques modeling absorbing (transmitting) boundary conditions, the extent of the finite spatial computational domain is simply chosen large enough to prevent reflected waves from affecting the cohesive response throughout the duration of numerical simulations. The powerful adaptive capabilities of the SDG model serve to mitigate the cost of this approach.

4.2.3. Regularized loading model

The far-field stress history is regularized to mitigate the computational expense of resolving sharp wavefronts. Specifically, $H(t)$ in (24) is replaced with a *regularized Heaviside function*, denoted by $\check{H}$, given by

$$\check{H}(t) = \begin{cases} -2(t')^3 + 3(t')^2 & : \quad t \le \tau_0, \\ 1 & : \quad \text{otherwise}. \end{cases} \tag{34}$$

The compressive tractions acting on the crack faces in the second LEFM subproblem are then $\bar{t}(t) = 2\check{H}(t)\bar{t}_\infty = \check{H}(t)\check{\sigma}$. Thus, the limiting normalized traction acting behind the crack tip is given by $\check{\sigma}(t)/\tilde{\sigma} = \check{H}(t)\sigma'$. Although the response to the regularized loading is very similar to that predicted by (31) nonetheless the crack-tip trajectory is computed for the LEFM model numerically, using the regularized load history with (25) and (28).

5. Numerical verification of CFM and LEFM analyses

This section compares numerical results for LEFM and CFM fracture responses, including crack tip trajectory and speed, energy release rate, and CPZ size, as a function of load-to-strength parameter $\sigma' = \check{\sigma}/\tilde{\sigma}$. It also verifies the SSY indicator proposed in Section 3.3. Since the entire cohesive surface debonds simultaneously when σ' exceeds unity, so that the apparent 'crack speed' is infinite, the focus is on problems where $0 < \sigma' < 1$. A low-amplitude load range, where $\sigma' \ll 1$, as well as a high-amplitude range, in which $\sigma' \to 1^-$ are studied. For the low-amplitude case, load data is used in the range $-3/2 \le \log\sigma' \le -1/2$, with equal logarithmic increments, and for the high-amplitude case, $\log\sigma' = -1/4, -1/8, -1/16, \cdots, -1/128$ is used, so that the largest value of σ' is $10^{-1/128} \approx 0.98$. In all cases, solution histories are plotted as functions of the normalized time, t', to facilitate comparison with the LEFM reference solution.

The solution from the CFM model is expected to match the LEFM reference solution, in the limit, as $\sigma' \to 0$, since this condition implies that $\lambda'_m \to 0$. The CFM solution is expected to deviate from the LEFM reference when the underlying assumptions that justify LEFM theory are invalid; in particular, when the SSY assumption does not hold. The a priori SSY indicator (20) should reliably predict whether the SSY condition is satisfied, but only if its underlying estimates for CPZ size and approximate equality between energy release rate and work of separation are both valid. This will be the case when the normalized crack speed, $\hat{v}/c_R$, changes slowly relative to the time required for the crack to extend a distance equal to the CPZ size. As a first approximation for the present example, (20) is evaluated with $\zeta = 9/16$ (cf. Section 5.3). Since, in this example, $\max_{t\in\mathcal{I}}(\check{\sigma}/\tilde{\sigma}) = \sigma'$, we obtain $\lambda'_m = 0.55$, which indicates that the SSY assumption is valid for most, if not all, of the low-amplitude-load range. In the high-amplitude range, the SSY indicator yields $1.76 \le \lambda'_m \le 5.36$, so it predicts that the SSY condition of LEFM is clearly violated. These predictions are tested against numerical results for the CFM model at the end of this section.

5.1. Crack-tip trajectory and velocity

Fig. 3 shows histories of the crack-tip velocity and position for the low-amplitude loads plotted against nondimensional time. The velocity histories for different values of σ' in the cohesive model are nearly identical, except at the onset of propagation. The reference LEFM solution exhibits visible differences with respect to the cohesive solutions at velocities larger than $0.6c_R$. However, these differences decrease as the crack-tip velocities approach their limiting value, c_R. Corresponding differences are observed in the crack-tip trajectories depicted in Fig. 3(b). The trajectories are nearly identical across the cohesive model simulations. The modest discrepancies between the CFM and LEFM crack velocities where $\dot{a} \approx 0.9c_R$ produce slightly larger crack extensions in the CFM results at later times. It is interesting to note that, although SSY is well satisfied (cf. Section 5.4), the other conditions that justified setting $\Gamma_0 = \tilde{\phi}$ in Section 4.1.2 are not met where the discrepancies occur; specifically, the crack-tip motion is highly unsteady and has not reached the asymptotic range where $\hat{v} \to c_R$. Overall, however, the agreement between the crack-tip motions predicted by the LEFM and CFM models is quite good for low-amplitude loads.

Let t_0 and v_0 denote, respectively, the time and velocity at the onset of crack propagation. Fig. 4 shows the crack speed and position during the early stages of crack growth. The initiation time for the LEFM solution is $t_0 \approx 1.5\tau_0$. The load regularization described in (34) causes a delay of about $\tau_0/2$ relative to the solution in (31). Although the initial crack velocity in the LEFM solution vanishes, it is observed that v_0 increases and τ_0 decreases as σ' increases in the CFM simulations. In fact, $t_0 \approx \tau_0$ for $\sigma' = 10^{-1/2}$; this corresponds to the time at which the sustained value of the applied load is attained in (34).

The crack-tip trajectories from the CFM simulations are very close to those from the LEFM solution at early times in Fig. 4(b). However, they start to deviate at later times due to the cumulative effect of the larger velocities in the CFM solutions. The difference grows as σ' increases.

Fig. 5 displays the response to high-amplitude loads. Crack propagation initiates almost immediately when the applied loading reaches its sustained value at time τ_0 in all of the CFM solutions; cf. (34). This contrasts with the LEFM theory, which, in general, predicts crack propagation at $t' = 1.5\tau_0$ corresponding to a delay of crack initiation by about $0.5\tau_0$. For low-amplitude loads, the delay time is the time required to develop the crack-tip singular fields.

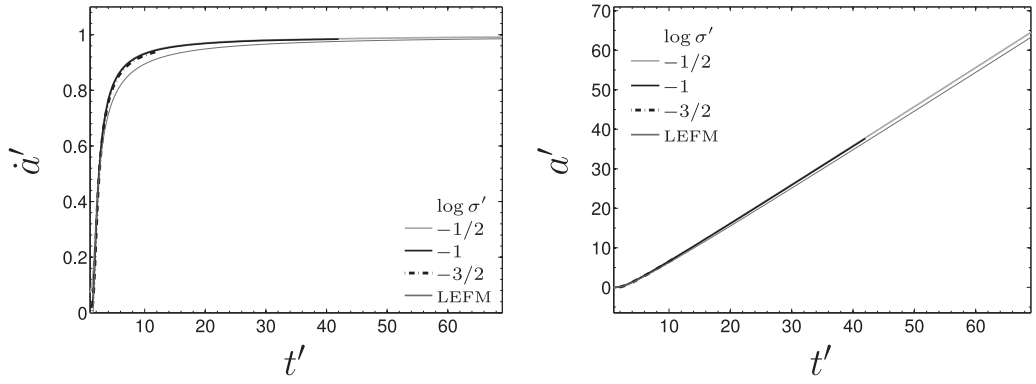

(a) Crack-tip velocity. (b) Crack-tip position.

Fig. 3. Crack-tip velocity histories and trajectories for low-amplitude loads, $\tilde{t}_\infty \ll \tilde{\sigma}$.

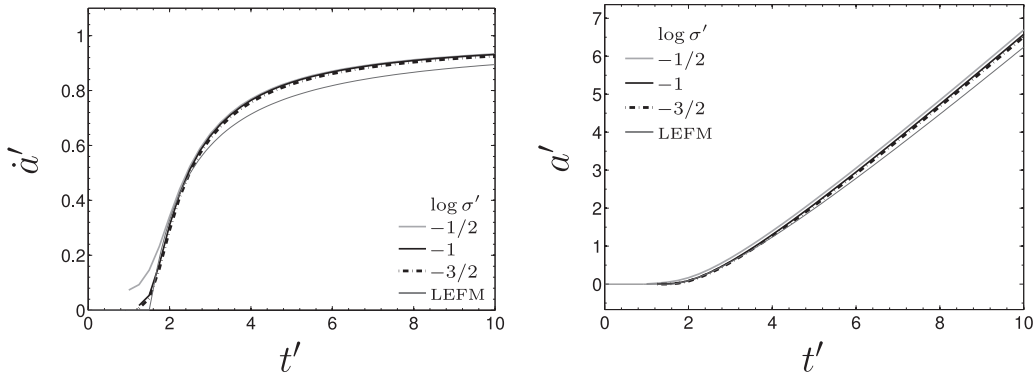

(a) Crack-tip velocity. (b) Crack-tip position.

Fig. 4. Early stages of crack-tip velocity histories and trajectories for low-amplitude loads, $\tilde{t}_\infty \ll \tilde{\sigma}$.

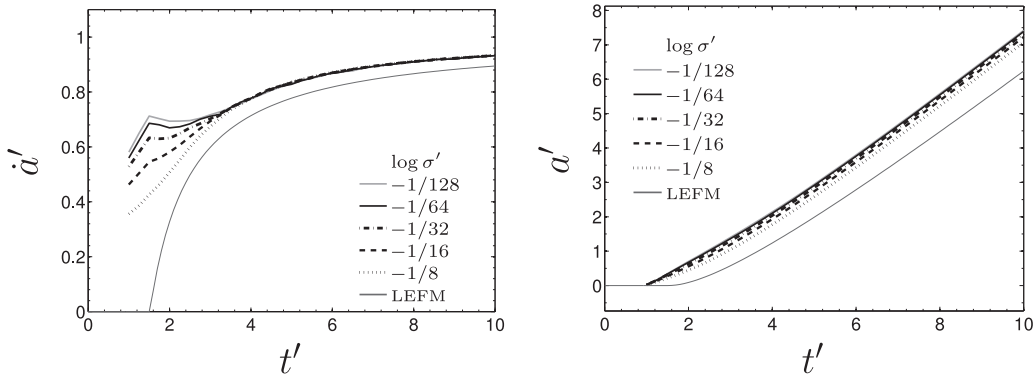

(a) Crack-tip velocity. (b) Crack-tip position.

Fig. 5. Crack-tip velocity histories and trajectories for high-amplitude loads, $\sigma' \to 1^-$.

However, for the high-amplitude loading considered here, where $\sigma' \approx 1$, the crack propagates almost immediately when the crack-surface loads reach their sustained value, even though the singular LEFM fields are not yet fully developed.

The initial velocity v_0 increases rapidly as $\sigma' \to 1^-$, and there are nonsmooth 'humps' in the CFM results at early times for these higher load intensities. Eventually, the CFM results for all load amplitudes collapse to the same curve as the crack speeds approach c_R. Numerical studies using variable ramp times in the load regularization (34), indicate that the hump feature is a numerical artifact of the regularization that becomes sharper and more prominent as the ramp time increases. Recalling that the regularization is simply a means to reduce computational expense, cf. Section 4.2.3, the hump feature is expected to become less pronounced and v_0 to increase as the regularization ramp time approaches zero. Apart from this numerical artifact, a general increase in v_0 and a greater discrepancy relative to the LEFM solution are observed as $\sigma' \to 1^-$ in the CFM model.

Fig. 5(b) shows the crack-tip trajectories for high-amplitude loading. Evidently, increasing σ' increases crack extension, as is

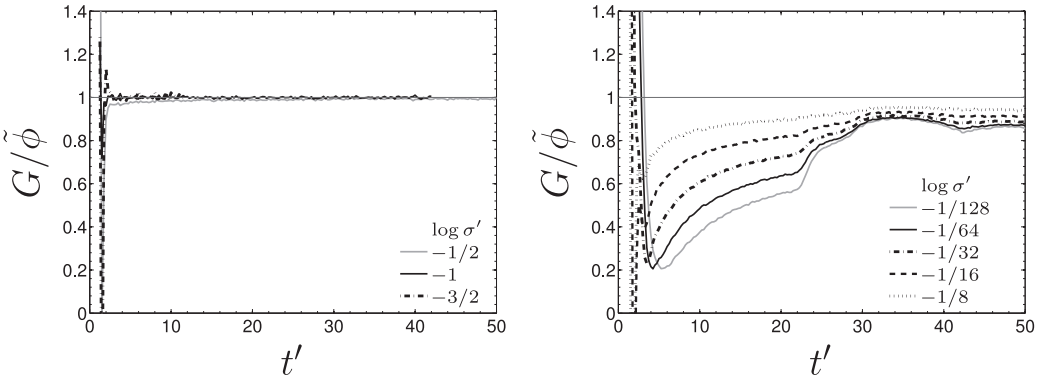

(a) Low-amplitude loading, $\bar{t}_\infty \ll \tilde{\sigma}$. (b) High-amplitude loading, $\bar{t}_\infty \to \tilde{\sigma}^-$.

Fig. 6. Evolution of energy release rate as a function of load amplitude.

expected for the larger crack-tip speeds. The LEFM crack extensions are smaller at any given time, due to the delayed initiation of crack growth and to the more gradual tip acceleration in the LEFM solution.

5.2. Energy release rate

Here the influence of load amplitude on the evolution of the energy release rate, G is investigated. As noted in Section 4.1.2, $G = \tilde{\phi}$ under steady-state conditions. Based on the discussion in Section 3.3 and on (16) and (17), it is concluded that transient effects become less important as the crack speed approaches c_R. However, this conclusion depends on the validity of the small-scale-yielding assumption, a condition in the derivation of (16), which, in turn, depends on the amplitude of the loading.

Fig. 6 shows the evolution of the energy release rate G as a function of load amplitude. The results for low-amplitude loading are shown in Fig. 6(a). It is observed that $G \approx \tilde{\phi}$ for $t \geq 2\tau_0 - 3\tau_0$. This corresponds to crack speeds $\dot{a} > 0.6c_R$ in Fig. 4(b). Highly unsteady crack growth and very small crack velocities cause the discrepancies between G and $\tilde{\phi}$ observed at early times when the impinging shock front releases energy across the entire cohesive surface, resulting in large values for G. This is followed by a brief excursion of G into the negative range. This is due to a rebound effect associated with the sudden load application, and numerical studies, not presented here, show that this effect reduces and eventually vanishes with increased ramp time in the load regularization. Afterwards, G quickly returns to and undergoes small oscillations about the work of separation, $\tilde{\phi}$. This is expected from (16) as the crack speeds are large and steadier in this range.

Fig. 6(b) demonstrates the changes in G when $\sigma' \approx 1^-$. The impinging planar wave causes a uniform separation along the entire cohesive surface. As $\sigma' \to 1^-$, this uniform separation approaches the critical separation, $\tilde{\delta}$, that corresponds to $\tilde{\sigma}$ in the Xu and Needleman TSR. This initial separation consumes a significant fraction of the total work of separation, leaving only the remaining fraction to be released during subsequent crack propagation. The fact that the steady values for G at $t \geq 40\tau_0$ decrease with increasing σ' is a consequence of this initial energy release and is characteristic of intrinsic cohesive models. The same effect can be discerned in Fig. 6(a), but to a much lesser extent due to the low-amplitude loading.

Similar to Fig. 6(a), it is observed that G decreases from values considerably larger than $\tilde{\phi}$ and after a short interval of negative value it raises to reach its steady state value. However, there is a rather prolonged interval before reaching the steady value. The main reason for this substantial difference between Fig. 6(a) and (b) is the validity of small-scale yielding condition assumed in (16).

5.3. Verification of cohesive process zone size estimate

In this section the performance of the process-zone size estimate (11) is examined. In Fig. 7, Λ/Λ^0 is presented as a function of normalized crack-tip velocity, comparing values computed by numerical simulation with estimates from (11) with $\zeta = 9/16$; cf. Section 2.2.4. There is a very good agreement between the numerical results for low-amplitude loading and the estimate (11) in Fig. 7(a), especially after the initial rapid crack acceleration. As explained in Section 2.2.4, a small change in $\hat{v}/c_R$ while the crack advances a distance Λ indicates nearly steady propagation. The crack velocity is small during the early stages of crack propagation; hence the process-zone size must be large based on (6) and (11). At the same time, the crack acceleration is relatively high, as shown in Fig. 4(a). Thus, in the early transient response it is found that the SSY condition is violated and the crack propagation is far from steady. These conditions undermine the estimate (11) and explain the small discrepancies between the numerical and estimated response at small crack speeds during the initial crack-tip acceleration. Overall, however, the estimate performs quite well over the full range of velocities for low-amplitude loading.

Fig. 7(b) shows results for high-amplitude loading, as $\sigma' \to 1^-$. The crack speed at crack initiation, v_0, is noticeably greater than zero, as shown in Fig. 5(a). Similar to the low-amplitude loading case, the condition of near-steady crack extension are violated during the early stages of crack propagation under high-amplitudes. However, now the SSY assumption is violated and the discrepancies between the computed process-zone size and the estimated values from (11) are significantly larger than those shown in Fig. 7(a). There is good agreement between the estimated and computed CPZ sizes only as $\dot{a} \to c_R$ because, under these conditions, $\Lambda \to 0$ so the evolution of $\hat{v}/c_R$ satisfies the near-steady propagation criterion given in Section 2.2.4. Overall, however, it is observed that CPZ-size estimate (11) is unreliable for high-amplitude loading.

Different choices for the value of ζ scale Λ/Λ^0 uniformly for all crack speeds, so the scaling of the estimates is somewhat arbitrary. Coincidently, Rice's suggested value for potential-based TSRs, $\zeta = 9/16$ (Rice, 1980), combines with the definition of CPZ-size given in Section 2.2.3 to make the estimate (11) very accurate, especially for low-amplitude loading. However, (11) is only intended to provide order-of-magnitude estimates, so the precise choice of ζ and the specific definition of the process-zone size are of little consequence.

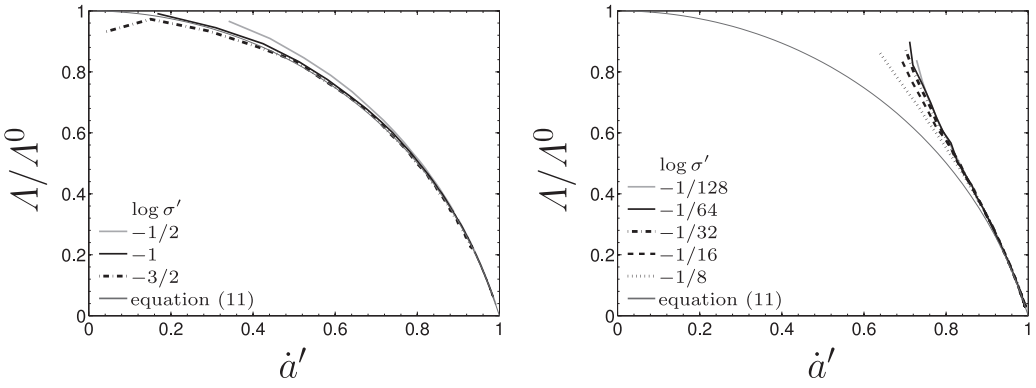

(a) Low-amplitude loading, $\bar{t}_\infty \ll \tilde{\sigma}$. (b) High-amplitude loading, $\bar{t}_\infty \to \tilde{\sigma}^-$.

Fig. 7. Study of cohesive-process-zone size for unsteady crack growth as a function of crack-tip velocity. Process zone sizes Λ, obtained from numerical computation for various load intensities, σ', are compared to the proposed estimate (11).

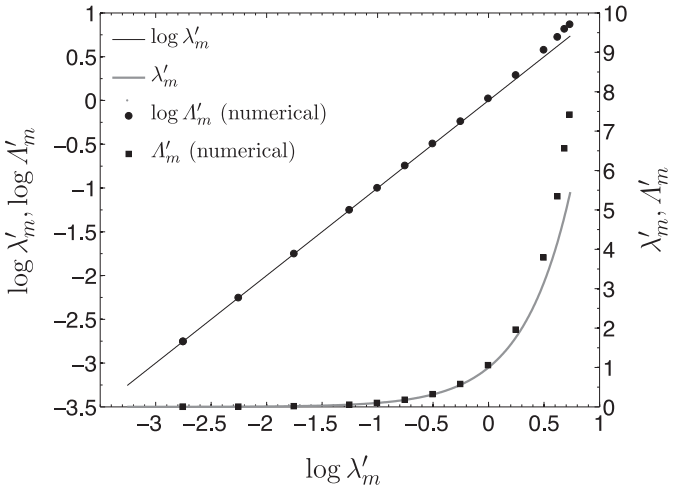

Fig. 8. Numerical verification of the SSY indicator (20); numerical values of Λ'_m are compared to the estimate λ'_m for various load intensities, σ'.

5.4. Verification of proposed SSY indicator

The results reported in Fig. 8 demonstrate the accuracy and effectiveness of the proposed SSY indicator, λ'_m; cf. (20). The same data is plotted twice in the figure, in log–log and log–normal formats, to expose the accuracy of the indicator as well as its effectiveness in revealing violations of the SSY condition. Eqs. (20), (24) and (34) are combined to obtain an analytical result for the SSY indicator, $\lambda'_m = \zeta\pi^2\sigma'^2$, represented as the continuous (line) curve in the plot. The discrete data for Λ'_m are computed, according to (19), using numerical values for Λ and $\check{r}$. The radius $\check{r}$ is directly computed by combining (4) and (12) with a finite difference approximation for $\hat{v}$, cf. (Abedi et al., 2009), and values of the stationary stress intensity factor are obtained by numerical integration of (25) using the regularized model for $\check{\sigma}(t)$ described in Section 4.2.3. Fig. 8 presents numerical results for Λ' using load intensities σ' between $10^{-7/4}$ and $10^{-1/128}$; the corresponding values of λ'_m range from 1.76×10^{-3} to 5.36. High-fidelity SDG solutions of the model problem are used to evaluate the CPZ-size, Λ, for each value of the load intensity, σ'. These numerical results are combined to obtain reference data for Λ'_m that are used to test the accuracy of the SSY indicator, λ'_m.

Ideally, the SSY indicator λ'_m should match Λ'_m throughout the entire range of load intensities. However, it is sufficient if the match only holds for load intensities up to and including the range where the SSY condition ceases to be satisfied. The log–log plot of the data exposes the accuracy of the SSY indicator, as indicated by the match between the continuous plot of $\log\lambda'_m$ and the discrete data for $\log\Lambda'_m$. Evidently, the error is extremely small for low-amplitude loads, and significant error only appears when λ'_m is greater than unity; *i.e.*, when $\Lambda > \check{r}$ which is well beyond the point where the SSY condition is first violated. Although nonconservative error ($\lambda'_m < \Lambda'_m$) is evident for larger load amplitudes, it is concluded that the SSY indicator is nonetheless accurate well beyond the range where it is needed. Furthermore, these errors are expected because the conditions that support the SSY indicator are violated in this range. Specifically, the SSY condition itself is violated, and the nearly steady crack growth condition is not satisfied, as shown in Fig. 7(b), causing (11) to produce an inaccurate estimate for the CPZ-size, Λ'. In addition, $G \approx \tilde{\phi}$ does not hold when $\sigma' \to 1^-$, cf. (15) and Fig. 6(b), and this violates another key assumption that was used to justify the SSY indicator, (20).

The log–normal plot of the data shows that the SSY indicator is effective in identifying the range of load amplitudes where the SSY condition ceases to be satisfied. It is observed that both λ'_m and Λ'_m are in close agreement and much smaller than unity until the condition (20) starts to be violated, say in the range where $\lambda'_m \approx 0.1$. Overall, (20) is shown to be an effective predictor of the range of load intensities where the SSY condition is satisfied in the CFM model and, therefore, where the LEFM theory is valid.

6. Conclusions

Given that macroscopic length scales can be unsuitable for characterizing the dynamic response of cohesive fracture models, the focus in this work was on the interplay between two crack-tip length scales that, together, provide useful insight into dynamic cohesive fracture models and their relation to LEFM. Expressions for modal stress singularity radii, $\check{r}_{(k)}$, are derived from LEFM theory and shown that they provide meaningful reference scales for normalizing the modal length scales of cohesive process zones, $\Lambda_{(k)}$. In particular, it was showed that the nondimensional CPZ sizes are $\Lambda'_{(k)} = \Lambda_{(k)}/\check{r}_{(k)} \approx \lambda'_{(k)} = \zeta_{(k)}\pi^2(\check{\sigma}_k/\tilde{\sigma}_{(k)})^2$, in which $\check{\sigma}_k$ are cohesive-traction scales and $\tilde{\sigma}_{(k)}$ are limiting values of modal crack-face tractions; cf. Section 3.1. Typically, $\tilde{\sigma}_{(k)}$ and $\check{\sigma}_k$ can be directly computed from the problem data; since $\check{\sigma}_k$ is proportional to the load-intensity measure, $\check{\sigma}$, $\lambda'_{(k)}$ in turn, proportional to the square of nondimensional load-to-strength parameter $\sigma' = \check{\sigma}/\tilde{\sigma}$.

In fact, the nondimensional load ratio σ' has threefold importance. First, the SSY indicator $\lambda'_{m\,(k)} \propto \sigma'^2$. Given that the individ-

ual factors, $\check{r}_{(k)}$ and especially $\Lambda_{(k)}$, cannot be easily estimated a priori, the proposed indicators $\lambda'_{m(k)}$ in (20) provide a practical means to verify the satisfaction of the SSY condition for dynamic LEFM solutions. Second, given that the nondimensional length ratio $\Lambda_{(k)}/\check{r}_{(k)} \propto \sigma'^2$ is related to ductile-to-brittle transition, the violation of SSY condition, *i.e.,* loss of validity of LEFM theory, implies a more ductile response. Finally, σ' is one of the fundamental nondimensional parameters associated with CFM. Accordingly, the effect of σ' on the cohesive response is of great importance as distinct values of σ' each represents a family of self-similar solutions. This analysis demonstrates how an increase to σ' corresponds to larger discrepancies between CFM and LEFM solutions. Thus, a parameter study on σ' both sheds light on CFM response and investigates the SSY assumption within LEFM theory.

It should be emphasized that satisfaction of the SSY condition and a good match between the LEFM and CFM crack-tip kinetics are both required for an accurate LEFM approximation to the nonlinear response. It is found that, although it performed quite well overall, the simple Griffith's criterion with constant specific energy used in this study was not completely consistent with the evolution of the energy release rate predicted by the CFM model. As a result, some discrepancies are found between the CFM and LEFM solutions, even for very small values of the SSY indicator. In short, LEFM theory underestimated various features of dynamic fracture, such as crack length and speed, even for low amplitude loading. These results underline the importance of the assumed crack-tip equation of motion in the LEFM model, a choice that merits careful consideration.

A parameter study in the variable σ' was performed to investigate a range of dynamic cohesive response for crack-tip trajectory and speed and to test the estimate of CPZ size and the proposed SSY indicator. The numerical study was restricted to mode-*I* loading in an unbounded domain, and the dynamic cohesive response was compared to a reference LEFM solution. In addition to providing a qualitative study of CFM response as a function of load intensity and a comparison with response according to LEFM theory, the numerical results verified key estimates for $\tilde{\phi}_{(k)}/G_{(k)}$ and CPZ-size that were used for the proposed SSY indicator. While the supporting estimates are not as reliable in general for high-amplitude loads, the numerical results demonstrate that they are nonetheless sufficient to support the SSY indicator (20) because they only lose validity after reaching load-intensity levels where SSY response no longer holds.

Several extensions to this work are possible. While the formulation applies to pure mode-*k* loading for any value of $k \in \{1, 2\}$, it would be worthwhile to extend the formulation and numerical investigations to address general mode mixity, including mode-*III*, in three dimensions. A problem of particular interest is mixed mode fracture in V-notched crack tips where s shown in Hills and Dini (2011), Cornetti et al. (2013) and Flicek et al. (2014) an intrinsic length scale arises under mixed mode crack propagation. The interplay of this length scale, LEFM singular radii, and CPZ sizes result in various interesting physics including in-plane fracture mode transition based on the ratio of these values and the magnitude of the applied loads. Finally, in a forthcoming paper, instead of stress-based length scales, velocity-singularity radii are derived for the transient dynamic case and are related to the *quasi-singular* velocity response observed in high-resolution numerical studies of CFM, as reported in (Abedi et al., 2009).

Supplementary materials

Supplementary material associated with this article can be found, in the online version, at doi:10.1016/j.ijsolstr.2016.10.007.

Appendix A. LEFM angular stress functions for a moving crack tip

Recalling the first terms of the asymptotic expansion of stress field of a moving crack tip (1), the representation of the angular functions $\Sigma_I^{ij}(\theta, \hat{v})$ and $\Sigma_{II}^{ij}(\theta, \hat{v})$ are modified from Freund (1990) such that mode *I* and *II* solutions can be expressed in a unified manner suitable for the modal analysis in Section 3,

$$\Sigma_I^{11} = -\frac{1}{D}\left\{(1+\alpha_{II}^2)^2 \frac{\cos\frac{1}{2}\theta_I}{\sqrt{\gamma_I}} - 4\alpha_I\alpha_{II}\frac{\cos\frac{1}{2}\theta_{II}}{\sqrt{\gamma_{II}}}\right\}, \tag{35a}$$

$$\Sigma_I^{12} = \frac{2\alpha_I(1+\alpha_{II}^2)}{D}\left\{\frac{\sin\frac{1}{2}\theta_I}{\sqrt{\gamma_I}} - \frac{\sin\frac{1}{2}\theta_{II}}{\sqrt{\gamma_{II}}}\right\}, \tag{35b}$$

$$\Sigma_I^{22} = \frac{1}{D}\left\{(1+\alpha_{II}^2)(1+2\alpha_I^2-\alpha_{II}^2)\frac{\cos\frac{1}{2}\theta_I}{\sqrt{\gamma_I}} - 4\alpha_I\alpha_{II}\frac{\cos\frac{1}{2}\theta_{II}}{\sqrt{\gamma_{II}}}\right\}, \tag{35c}$$

and

$$\Sigma_{II}^{11} = \frac{2\alpha_{II}(1+\alpha_{II}^2)}{D}\left\{\frac{\sin\frac{1}{2}\theta_I}{\sqrt{\gamma_I}} - \frac{\sin\frac{1}{2}\theta_{II}}{\sqrt{\gamma_{II}}}\right\}, \tag{36a}$$

$$\Sigma_{II}^{12} = \frac{1}{D}\left\{4\alpha_I\alpha_{II}\frac{\cos\frac{1}{2}\theta_I}{\sqrt{\gamma_I}} - (1+\alpha_{II}^2)^2\frac{\cos\frac{1}{2}\theta_{II}}{\sqrt{\gamma_{II}}}\right\}, \tag{36b}$$

$$\Sigma_{II}^{22} = -\frac{2\alpha_{II}}{D}\left\{(1+2\alpha_I^2-\alpha_{II}^2)\frac{\sin\frac{1}{2}\theta_I}{\sqrt{\gamma_I}} - (1+\alpha_{II}^2)\frac{\sin\frac{1}{2}\theta_{II}}{\sqrt{\gamma_{II}}}\right\}, \tag{36c}$$

in which

$$\alpha_{(k)} = \sqrt{1-\hat{v}^2/c_{(k)}^2} \tag{37a}$$

$$\gamma_{(k)} = \sqrt{1-(\hat{v}\sin\theta/c_{(k)})^2} \tag{37b}$$

$$\tan\theta_{(k)} = \alpha_{(k)}\tan\theta, \quad k = 1, 2, \tag{37c}$$

$$D = 4\alpha_I\alpha_{II} - (1+\alpha_{II}^2)^2. \tag{37d}$$

The reference velocities, $c_I := c_d$ and $c_{II} := c_s$, are the dilatational and shear wave speeds, which for an isotropic, linearly elastic material with Lamé parameters, λ and μ, and mass density ρ, are given by

$$c_d = \sqrt{\frac{\lambda+2\mu}{\rho}}, \quad c_s = \sqrt{\frac{\mu}{\rho}}. \tag{38}$$

It can be shown that the *Rayleigh wave speed*, denoted by c_R, equals the non-zero value of $\hat{v}$ at which D vanishes (Rayleigh, 1885).

It is customary to decorate α, θ and γ with d and s, similarly to c_d and c_s. However, the indices 1 and 2 are used instead, since the displacements for dilatational and shear waves are mainly in the x_1 and x_2 directions, respectively. Many relations, such as (37c), can be written in a more compact form when expressed with this convention.

References

Abedi, R., 2010. Spacetime Damage-Based Cohesive Model for Elastodynamic Fracture with Dynamic Contact. Ph.D. thesis. Department of Theoretical and Applied Mechanics, University of Illinois at Urbana–Champaign.

Abedi, R., Haber, R., 2011. Spacetime dimensional analysis and self-similar solutions of linear elastodynamics and cohesive dynamic fracture. Int. J. Solids Struct. 48 (13), 2076–2087.

Abedi, R., Haber, R.B., Petracovici, B., 2006. A spacetime discontinuous Galerkin method for elastodynamics with element-level balance of linear momentum. Comput. Methods Appl. Mech. Eng. 195, 3247–3273.
Abedi, R., Haber, R.B., Thite, S., Erickson, J., 2006. An *h*–adaptive spacetime–discontinuous Galerkin method for linearized elastodynamics. Revue Européenne de Mécanique Numérique (Eur. J. Comput. Mech.) 15 (6), 619–642.
Abedi, R., Hawker, M.A., Haber, R.B., Matouš, K., 2009. An adaptive spacetime discontinuous galerkin method for cohesive models of elastodynamic fracture. Int. J. Numer. Methods Eng. 1, 1–42.
Anderson, T.L., 2005. Fracture Mechanics: Fundamentals and Applications. CRC Press, Portland.
Barenblatt, G.I., 1962. The mathematical theory of equilibrium of cracks in brittle fracture. Adv. Appl. Mech. 7, 55–129.
Carpinteri, A., Cornetti, P., Barpi, F., Valente, S., 2003. Cohesive crack model description of ductile to brittle size-scale transition: dimensional analysis vs. renormalization group theory. Eng. Fract. Mech. 70 (14), 1809–1839.
Cornetti, P., Sapora, A., Carpinteri, A., 2013. Mode mixity and size effect in v-notched structures. Int. J. Solids Struct. 50 (10), 1562–1582.
Cornetti, P., Sapora, A., Carpinteri, A., 2014. T-stress effects on crack kinking in finite fracture mechanics. Eng. Fract. Mech. 132, 169–176.
Dodds Jr, R.H., Anderson, T.L., Kirk, M.T., 1991. A framework to correlate a/w ratio effects on elastic-plastic fracture toughness (j c). Int. J. Fract. 48 (1), 1–22.
Dugdale, D.S., 1960. Yielding of steel sheets containing slits. J. Mech. Phys. Solids 8, 100–104.
Flicek, R., Hills, D., Dini, D., 2014. Refinements in the characterisation of mode-mixity and small scale yielding at sharp notch roots. Eng. Fract. Mech. 126, 73–86.
Freund, L., 1973. Crack propagation in an elastic solid subjected to general loading - 3. stress wave loading.. J. Mech. Phys. Solids 21 (2), 47–61.
Freund, L.B., 1990. Dynamic Fracture Mechanics. Cambridge University Press, Cambridge, UK.
Harder, N., 1991. Dimensional analysis for concrete in fracture. Materiaux et Constructions 24 (141), 202–209.
Hills, D., Dini, D., 2011. Characteristics of the process zone at sharp notch roots. Int. J. Solids Struct. 48 (14–15), 2177–2183.
Jin, Z.-H., Sun, C., 2005. Cohesive fracture model based on necking. Int. J. Fract. 134 (2), 91–108.
Jin, Z.-H., Sun, C., 2006. A comparison of cohesive zone modeling and classical fracture mechanics based on near tip stress field. Int. J. Solids Struct. 43 (5), 1047–1060.
Pandolfi, A., Krysl, P., Ortiz, M., 1999. Finite element simulations of ring expansion and fragmentation: the capturing of length and time scales through cohesive models of fracture. Int. J. Fract. 95, 279–297.
Rayleigh, L., 1885. On waves propagated along the plane surface of an elastic solid. Proc. R. Soc. London A 17, 4–11.
Rice, J., 1968. Mathematical Analysis in the Mechanics of Fracture. In: Liebowitz, H. (Ed.), Fracture, an Advanced Treatise, 2. Academic Press, New York, United States, pp. 191–311.
Rice, J., 1980. The Mechanics of Earthquake Rupture. In: Physics of the Earth's Interior. North-Holland Publ. Co.: Amsterdam, Italian Physical Society, pp. 555–649.
Xu, X.P., Needleman, A., 1994. Numerical simulations of fast crack growth in brittle solids. J. Mech. Phys. Solids 42, 1397–1434.
Yu, H., Suo, Z., 2000. Intersonic crack growth on an interface. Proc. R. Soc. 456 (1993), 223–246.
Yu, H.H., Suo, Z., 2000. Intersonic crack growth on an interface. Proc. R. Soc. London, Series A (Mathematical, Physical and Engineering Sciences) 456 (1993), 223–246.